

COSMOLOGICAL CONSTRAINTS FROM THE REDSHIFT DEPENDENCE OF THE GALAXY ANGULAR 2-POINT CORRELATION FUNCTION

XIAO-DONG LI,

School of Physics, Korea Institute for Advanced Study, 85 Heogiro, Dongdaemun-gu, Seoul 130-722, Korea

CHENG CHENG,

Kavli Institute for Theoretical Physics China, Institute of Theoretical Physics, Chinese Academy of Sciences, Zhong Guan Cun Street 55#, Beijing, 100190, P.R. China and
 University of Chinese Academy of Sciences, P.R. China

CHANGBOM PARK,

School of Physics, Korea Institute for Advanced Study, 85 Heogiro, Dongdaemun-gu, Seoul 130-722, Korea

CRISTIANO G. SABIU, HYUNBAE PARK,

Korea Astronomy and Space Science Institute, Daejeon 305-348, Korea

JUHAN KIM¹,

Center for Advanced Computation, Korea Institute for Advanced Study, 85 Hoegi-ro, Dongdaemun-gu, Seoul 130-722, Korea and
 School of Physics, Korea Institute for Advanced Study, 85 Heogiro, Dongdaemun-gu, Seoul 130-722, Korea

AND

SUNGWOOK E. HONG

School of Physics, Korea Institute for Advanced Study, 85 Heogiro, Dongdaemun-gu, Seoul 130-722, Korea

Draft version September 7, 2016

ABSTRACT

We use the shape of galaxy 2-point correlation function to measure the redshift dependence cosmology volume effect. ...

Keywords: large-scale structure of Universe — dark energy — cosmological parameters

1. INTRODUCTION

Dark energy ... Large scale structure...

2pCF is a good statistic... blahblah In 2d xi(s,μ)
 ... In *** we used the redshift dependence of 2pCF to probe the volume and AP effect... The method is applied to BOSS data in *** and obtain tight constraint...

In *** we further propose to use the shape of xi(s) to probe the volume effect... Stretch or compression shifts the clustering properties in some particular scale to larger or smaller scales... The shape of measured xi(s) is thus stretched or compressed.

The outline of this paper is as follows.

This paper is organized as follows... The outline of this paper proceeds as follows. In §2 we briefly review the nature and consequences of the AP effect and volume changes when performing coordinate transforms in a cosmological context. In §3 we describe the N-body simulations and mock galaxy catalogues that are used to test our methodology. In §4, we describe our new analysis method for quantifying the redshift dependence of volume effect. We conclude in §5.

2. GEOMETRIC DEFORMATION WHEN

In this section we briefly introduce the scaling effect caused by wrongly assumed cosmological parameters. A more detailed description has been provided in Li et al. (2014, 2015, 2016).

Suppose that we are probing the size of some objects

in the Universe. We measure its redshift span Δz and angular size $\Delta\theta$, then compute its sizes in the radial and transverse directions using the following formulas

$$\Delta r_{\parallel} = \frac{c}{H(z)} \Delta z, \quad \Delta r_{\perp} = (1+z) D_A(z) \Delta\theta, \quad (1)$$

where H is the Hubble parameter and D_A is the angular diameter distance. In the particular case of a flat universe composed by a cold dark matter component and a constant EoS dark energy component, they take the forms of

$$H(z) = H_0 \sqrt{\Omega_m a^{-3} + (1 - \Omega_m) a^{-3(1+w)}}, \\ D_A(z) = \frac{1}{1+z} r(z) = \frac{1}{1+z} \int_0^z \frac{dz'}{H(z')}, \quad (2)$$

where $a = 1/(1+z)$ is the cosmic scale factor, H_0 is the present value of Hubble parameter and $r(z)$ is the comoving distance.

In case wrong values of Ω_m and w are adopted, the inferred Δr_{\parallel} and Δr_{\perp} are wrong, resulting in wrong estimation in the object's shape (AP effect) and size (volume effect). These effects and their cosmological consequences have been investigated in Li et al. (2014, 2015, 2016).

In this paper we focus on the mis-estimation of the angular size Δr_{\perp} . The ratio of mis-estimation is

$$\alpha_{\perp} \equiv \frac{\Delta r_{\perp, \text{wrong}}}{\Delta r_{\perp, \text{true}}} = \frac{D_{A, \text{wrong}}}{D_{A, \text{true}}}, \quad (3)$$

¹ Corresponding Author: kjhan@kias.re.kr

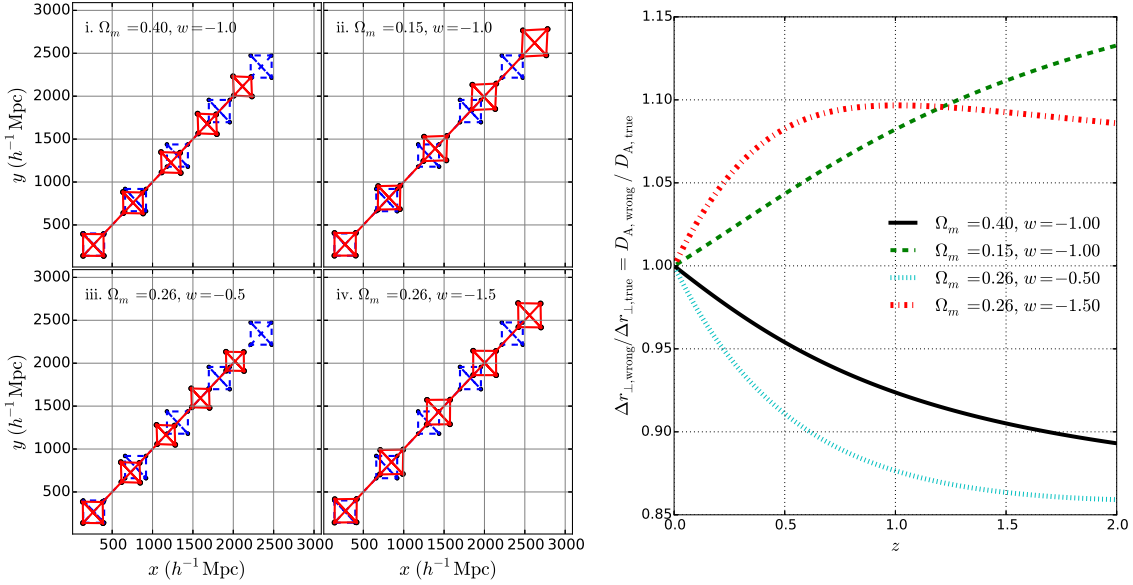


Figure 1. The scaling in four wrongly assumed cosmologies ..., assuming a true cosmology of $\Omega_m = 0.26$, $w = -1$. Left panel shows a series objects distributes as five perfect squares, measured by an observer located at the origin. Their true positions and shapes are plotted in blue dashed lines. The observer measures the redshifts of these objects, adopts the wrong cosmologies to compute the distance, and obtains wrong results (red solid lines). Right panel shows the mis-estimation of angular diameter distance when the wrong cosmologies are adopted.

where ‘‘true’’ and ‘‘wrong’’ denote the values of D_A in the true cosmology and wrongly assumed cosmologies, respectively.

An illustration is provided in the left panels of Figure 1. Suppose that the true cosmology is a flat Λ CDM with present matter ratio $\Omega_m = 0.26$ and standard dark energy EoS $w = -1$. If we were to distribute a series of perfect squares at various distances ranging from 500 Mpc/h to 3000 Mpc/h, and an observer located at the origin were to measure their redshifts and infer the sizes of the squares using the distance-redshift relations of four incorrect cosmologies

- (i). $\Omega_m = 0.40$, $w = -1.0$,
- (ii). $\Omega_m = 0.15$, $w = -1.0$,
- (iii). $\Omega_m = 0.26$, $w = -0.5$,
- (iv). $\Omega_m = 0.26$, $w = -1.5$,

as a result, the shapes of the squares appear distorted (AP effect), and their sizes are wrongly estimated (volume effect). Cosmological models (i,iii) yield to compressed size (in both angular and LOS direction), and the degree of compression increases with increasing distance;

The mis-estimation of angular size, $\Delta r_{\perp,\text{wrong}} / \Delta r_{\perp,\text{true}}$, are displayed in the right panel of Figure 1. All cosmologies, $\Delta r_{\perp,\text{wrong}} / \Delta r_{\perp,\text{true}}$ evolves a lot in the redshift range $0 < z < 2$. As an example, when adopting the quintessence cosmology $\Omega_m = 0.26$, $w = -0.5$, the angular size is underestimated by 8.9%, 12.3%, 13.6%, 14.1% at $z = 0.5, 1, 1.5, 2$.

In sum, as a consequence of incorrectly adopted cosmologies, the size of the objects is mis-estimated and the magnitude of mis-estimation depends on the redshift. In this paper we use the galaxy angular 2pCF to probe the mis-estimation of angular size $\Delta r_{\perp,\text{wrong}} / \Delta r_{\perp,\text{true}}$.

3. THE SIMULATION DATA

We test the method on the Horizon Run 4 (HR4) simulation (Kim et al. 2015). HR4 used $N = 6300^3$ particles in a box size of $L = 3150 h^{-1}\text{Mpc}$. It adopted the second order Lagrangian perturbation theory (2LPT) initial conditions at $z_i = 100$ and a WMAP5 cosmology $(\Omega_b, \Omega_m, \Omega_\Lambda, h, \sigma_8, n_s) = (0.044, 0.26, 0.74, 0.72, 0.79, 0.96)$ (Komatsu et al. 2011). The particle mass is $\simeq m_p \simeq 9.02 \times 10^9 h^{-1}\text{M}_\odot$.

Mock galaxy samples are produced from the simulation based on a modified one-to-one correspondence scheme (Hong et al. 2016). The most bound member particles (MBPs) of simulated halos are adopted as the tracer of galaxies, and the merger timescale is computed to get the lifetime of merged halos. Merger trees of simulated halos are constructed by tracking their MBPs from $z = 12$ to 0. When a merger event occurs, we adopt the formula of Jiang et al. (2008) to calculate the merger timescale and determine when a satellite galaxy is completely disrupted.

Hong et al. (2016) compared the 2pCF of the SDSS DR7 volume-limited galaxy sample (Zehavi et al. 2011) and the HR4 $z = 0$ mock galaxies. The mock galaxies shows a similar finger of god (FOG) feature (Jackson 1972) as the observation. On scales greater than $1 h^{-1}\text{Mpc}$., the projected 2pCF of the mock and observational samples agree within 1σ deviation.

The output of HR4 simulation includes one all-sky light cone mock galaxy catalogue reaching $r = 3150 h^{-1}\text{Mpc}$ and a series (**how many?**) of snapshot mock galaxy catalogues at different redshifts. In this paper we use five snapshot data at $z = 0, 0.5, 1, 1.5, 2$. We require subhalos to have at least 30 member particles, so the minimal mass of galaxies is $\simeq m_p \simeq 2.7 \times 10^{11} h^{-1}\text{M}_\odot$. At the five redshifts, we get a number of 457, 406, 352, 206 and 228 million mock galaxies, corresponding to a number density of 1.46, 1.30, 1.13, 0.98 and 0.73 in unit of $10^{-2} h^3 \text{Mpc}^{-3}$, respectively.

4. GALAXY ANGULAR 2PCF

4.1. Galaxy distribution at different redshifts

The left panels of Figure 2 show the x, y coordinates of galaxies in a $260h^{-1}\text{Mpc} \times 130h^{-1}\text{Mpc} \times 105h^{-1}\text{Mpc}$ volume, taken from the five snapshots. The gravitational growth of structures with decreasing redshift is clearly shown. We display all mock galaxies with $M > 3.0 \times 10^{11}h^{-1}\text{M}_\odot$. At lower redshift, galaxies become more massive, so they are more galaxies satisfying the threshold.

If one adopts a wrong cosmology to compute galaxy positions, there would be a scaling of the galaxy distribution. In the left panel we show the case when a wrong set of parameters $\Omega_m = 0.05, w = -1.5$ is assumed, leading to large upscaling of 25.6%, 47.3%, 62.2%, 71.7% at redshifts $z = 0.5, 1.0, 1.5, 2.5$.

Compared with the true galaxy distribution, the apparent distribution inferred by wrong set of parameters show clear evolution with redshift due to the different scaling at different redshifts. In case of Figure 2, the apparent size of large scale structures increases with redshift.

The growth of structure also make the size of structures evolves with redshift. In the next subsection we will discuss how to distinguish these two effects in the galaxy angular 2pCF.

4.2. Galaxy angular 2pCF: amplitude and shape at different redshifts

The left panel of Figure 3 displays the measured angular 2pCF of galaxies (multiplied by scale r) in the five snapshot.

The amplitude of 2pCF is crucially affected by the cosmic structure growth and the galaxy bias. We find $\xi(z=0) > \xi(z=0.5) > \xi(z=1)$. At low redshift, the large scale structures experienced most gravitational growth, leading to stronger clustering strength and higher amplitude of 2pCF. On the contrary, at higher redshift we find $\xi(z=2) > \xi(z=1.5) > \xi(z=1)$, simply because by applying a uniform mass cut we are selecting more biased galaxies at higher redshift.

Different from the large variation of amplitude among the different redshifts, the shape of 2pCF maintains similar at all redshifts. At all redshifts, we see the $r\xi$ peaks at $r \sim 9h^{-1}\text{Mpc}$, and monotonically drops at larger or smaller scales. The only exception is the relative enhancement of 2pCF at $r \lesssim 2h^{-1}\text{Mpc}$, which is caused by the non-linear growth of structures on small scales and becomes more dramatic at lower redshift.

The middle panel of Figure 3 displays the $r\xi$ normalized by the overall amplitude within $5h^{-1}\text{Mpc} < r < 50h^{-1}\text{Mpc}$ (here after $\hat{r}\xi$). The nice overlapping of the results from five redshifts suggests small evolution of shape with redshift. In the right panel, we compare the high redshift $\hat{r}\xi$ to the $z=0$ result. There is 1-4% relative enhancement at $r < 10h^{-1}\text{Mpc}$, and < 1.5% relative suppression at $r > 25h^{-1}\text{Mpc}$. The trend is monotonic with redshift.

In all, we conclude that the shape of the 2pCF is more robust than the amplitude against redshift and galaxy bias.

4.3. Galaxy angular 2pCF: in wrong cosmologies

When a wrong set of cosmological parameters is adopted, the galaxy distribution is artificially scaled.

This scaling is expected to change the shape of the 2pCF, following the relationship,

$$\hat{\xi}_{\text{wrong}}(r) = \hat{\xi}_{\text{true}}(\alpha_{\perp} r), \quad (4)$$

a simple consequence of the fact that clustering patterns at distance r now appears on a the scale $\alpha_{\perp} r$. The redshift evolution of α_{\perp} leads to redshift evolution of shape.

Lower panels of Figure 3 shows the $r\xi$ in five snapshots, in case that the cosmology $\Omega_m = 0.05, w = -1.5$ is adopted to construct the galaxy distribution (the right panels of Figure 2). The middle panel displays the clear redshift evolution of shape of $r\xi$. E.g., from $z=0$ to $z=2$, the peak location is shifted from $r = 9h^{-1}\text{Mpc}$ to $r \sim 15h^{-1}\text{Mpc}$ at $z=2$ since the angular separation is upscaled by 71.7%.

The right panel shows that, at higher redshift, there is a 20-40% change in the value of $\hat{r}\xi$.

The amplitude of $r\xi$ is amplified due to the stretch of scale. As shown in the left panel, the amplitude monotonically increases as a function of redshift. But this phenomenon can also appear in case of gravitational growth of structure or increasing of bias, so we will not make use of it to do cosmological constraint. We utilize the redshift evolution of the 2pCF shape as a signal suggesting that the assumed cosmological parameters are wrong.

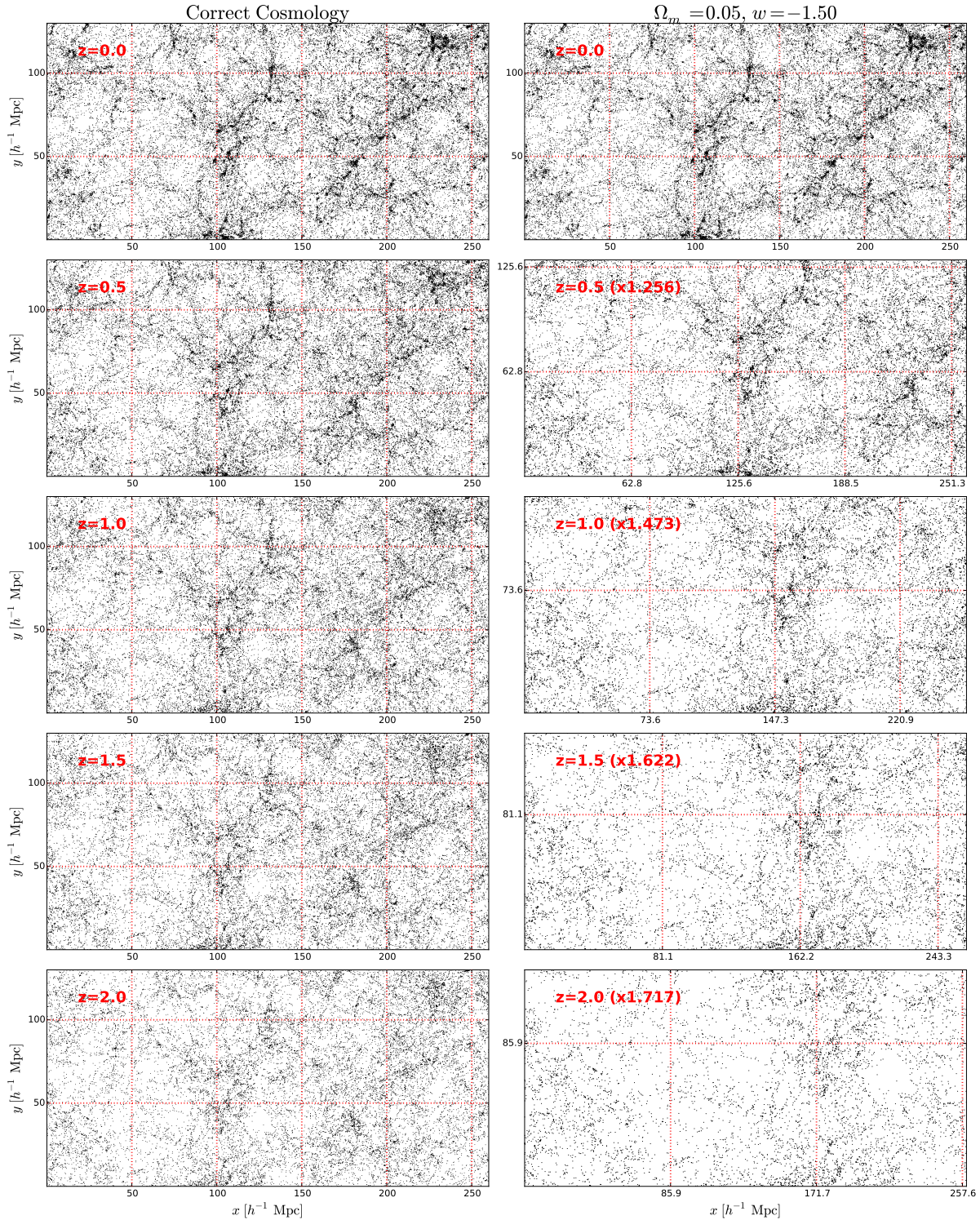
In Figure 5 we further plot the redshift evolution of 2pCF in the four wrong cosmologies of Figure 1. In all cases, the scaling leads to evident redshift evolution of the shape of $r\xi$. When the cosmologies $\Omega_m = 0.4, w = -1$ and $\Omega_m = 0.26, w = -0.5$ are adopted, the compression of structure makes the clustering patterns appears on smaller scales. This leads to “steeper” slope of $r\xi$, and the higher the redshift, the steeper the slope. To the opposite, when adopting the cosmologies $\Omega_m = 0.15, w = -1$ and $\Omega_m = 0.26, w = -1.5$, the stretch of size makes the slope shallower at higher redshifts.

4.4. Systematic effects

The same as Li et al. (2014, 2015, 2016) we need to correct for the redshift evolution of $r\xi$ caused by effects other than the cosmological effect.

Figure 3 already shows that, the growth of structure, especially in low redshift and on non-linear scales, changes the shape of $r\xi$ and caused relative enhancement on $r \lesssim 2h^{-1}\text{Mpc}$. So we limit the region of scale to $r > 5h^{-1}\text{Mpc}$ to minimize its effect.

Galaxies are biased tracers of dark matter field, and more massive galaxies tend to reside in regions with higher density contrast. So in large scale structure surveys the bias of the galaxy sample is an important factor which has large effect on the clustering properties of the sample. The upper panels of Figure 4 displays five set of galaxy samples in a $3175 \times 3175 \times 105 (h^{-1}\text{Mpc})^3$ volume, taken from the $z=0$ snapshots data. Different lower mass limits of $3 \times 10^{11} M_\odot, 3 \times 10^{11} M_\odot, 3 \times 10^{11} M_\odot$ and $3 \times 10^{11} M_\odot$ are imposed to create subsamples with different galaxy bias, and the measured angular 2pCF are displayed. The different mass cuts result in large variation in the amplitude of the 2pCF (left panel), while the shape of the 2pCF remains less affected (middle panel). Compared with the sample with mass cut $M > 3 \times 10^{11} M_\odot$, samples with mass limit $3 \times 10^{11} M_\odot, 3 \times 10^{11} M_\odot$ and $3 \times 10^{11} M_\odot$ have the amplitude of 2pCFs enhanced by 10%, 50% and 100%, while the change in $\hat{r}\xi$ is only

**Figure 2.** blah

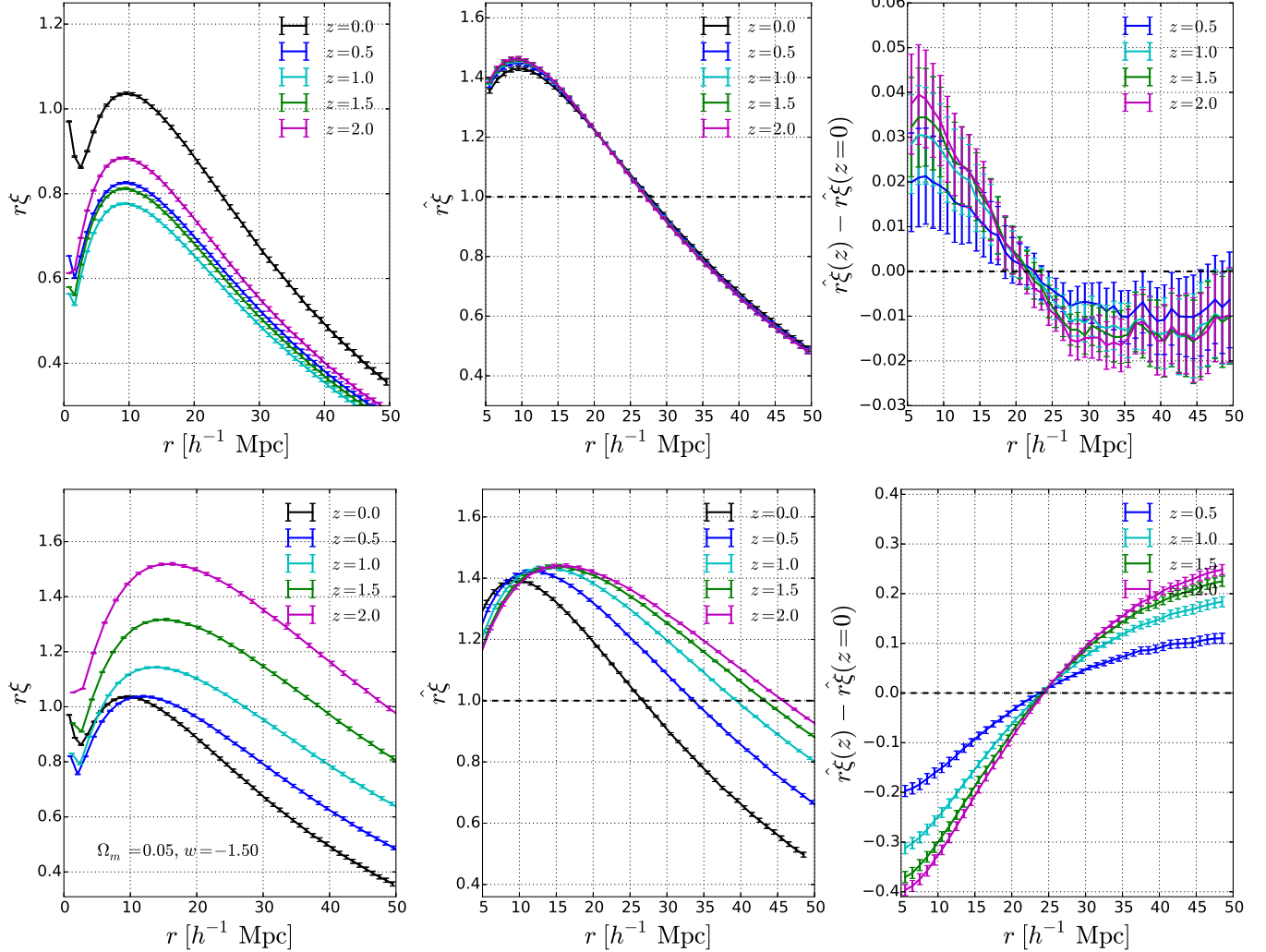


Figure 3. 2pCF at different redshifts.

0.5%, 2% and 4%. Considering the very large change in the mass cut, the change in the shape of 2pCF is not significant.

The galaxy peculiar velocity contribute to the observed galaxy redshift and distorted the galaxy radial position in redshift space, known as the redshift space distortion (RSD). It is the major source of systematics for our analysis of Li et al. (2014, 2015, 2016), where the 3D galaxy distribution is utilized to derive cosmological constraint. In this analysis its effect becomes much milder since the angular positions of the galaxies is not affected by RSD at all. But it still affects our analysis in the procedure of preparing the subsamples of galaxies for 2pCF analysis. The galaxies observed in a survey are split into shells of subsamples, with different redshift ranges, to get the 2pCF at different redshifts. RSD distorts the galaxy redshift and as a result some galaxies close the boundaries of shells will be distributed to wrong redshift shells.

The lower panel of Figure 4 displays the RSD effect on 2pCF. To mimick the effect of RSD we shift the Z coordinates of galaxies according to the relation

$$\Delta z = (1+z) \frac{v_Z}{c}, \quad (5)$$

where v_Z is the galaxy peculiar velocity in Z direction. Then we split the whole box into 30 slices with thickness $105h^{-1}\text{Mpc}$, and measure the angular 2pCF. The left panel shows that the amplitude of measured 2pCF is enhanced by $\sim 10\%$ in case of considering the RSD effect on splitting samples. The middle panel shows that the shape of 2pCF is also altered – the slop is suppressed. If looking at the redshift evolution, the curves $\hat{r}\xi - \hat{r}\xi(z=0)$ displayed in the right panel, they changed a lot compared with the case of no RSD effect (the right panel of Figure 3), but do not become much larger.

Similar to RSD, the redshift errors in survey can affect the subsamples of galaxies by buring the boundaries of shells. This effect should be properly quantified, especially in case of a photometric survey where the redshift uncertainty can be $\Delta z \approx 0.02$.

In Li et al. (2014, 2015, 2016), the systematic effects contributing to the redshift evolution of galaxy clusterings are modeled in mock surveys and subtracted. Similar treatment could be conducted here. One shall construct mock surveys with the above effects included for the correction of systematics.

4.5. Likelihood Analysis

We build up a likelihood function to describe how significant is the redshift evolution of the 2pCF shape, so that to determine whether the adopted cosmological parameters are correct. The redshift evolution is characterized by the difference between the $\hat{r}\xi$ measured in the lowest redshift and higher ones; the cosmology having least redshift evolution of $\hat{r}\xi$ is considered to be the most plausible one and has smallest χ^2 . So we have

$$\chi^2 \equiv \sum_{i=2}^{n_z} \sum_{j_1=1}^{n_r} \sum_{j_2=1}^{n_r} \mathbf{p}(z_i, r_{j_1}) (\mathbf{Cov}_i^{-1})_{j_1, j_2} \mathbf{p}(z_i, r_{j_2}), \quad (6)$$

where n_z is the number of redshifts, is number of bins in $\hat{r}\xi(r)$; in this analysis we have five redshift bins, and 35 r bins with bin width $1h^{-1}\text{Mpc}$ in the range $5h^{-1}\text{Mpc} < r < 40h^{-1}\text{Mpc}$. $\mathbf{p}(z_i, r_j)$ is the redshift

evolution of clustering, $\hat{r}\xi$, with systematic effects subtracted

$$\mathbf{p}(z_i, r_j) \equiv \delta \hat{r}\xi(z_i, z_1, r_j) - \delta \hat{r}\xi_{\text{sys}}(z_i, z_1, r_j) \quad (7)$$

\mathbf{Cov}_i is the covariance matrix.

It is difficult to conduct the 2pCF of the whole snapshot box with hundreds of millions of galaxies. We split the box into 120 subsamples with X, Y, Z sizes of $1575h^{-1}\text{Mpc}$, $1575h^{-1}\text{Mpc}$, $105h^{-1}\text{Mpc}$ and measure the angular 2pCF in the $X-Y$ plan in these subsamples. The average of the 2pCFs are taken as the 2pCF of the whole box. The covariance matrix is also estimated from these 2pCFs.

In real observations we observe *different* objects at different redshift shells. To mimick this when calculating the redshift evolution of 2pCF we use subsamples at different positions at different redshifts. E.g., if for the $z = 0$ snapshot we use the $\hat{r}\xi$ measured in the subsample $0h^{-1}\text{Mpc} < Z < 105h^{-1}\text{Mpc}$, at higher redshifts we adopt the $\hat{r}\xi$ measured in a subsample $105h^{-1}\text{Mpc} < Z < 210h^{-1}\text{Mpc}$, and take the difference between them to get $\delta \hat{r}\xi$. So we are always comparing 2pCF measured from different samples of galaxies. If simply comparing the 2pCF of a same sample of galaxies at different redshifts, one would significantly underestimate the statistical uncertainty of $\delta \hat{r}\xi$ by ignoring the cosmic variance².

Figure 5 displayed the 2pCF measured in the four cosmologies displayed in Figure 1. For the cosmologies $\Omega_m = 0.4, w = -1$ and $\Omega_m = 0.26, w = -0.5$, the compression of structure rescale large scale clustering patterns into small scales; the compression becomes more significant at higher redshift. In these cosmologies we get 2pCFs with steeper slope and, the higher redshift, the steeper. For $\Omega_m = 0.15, w = -1$ and $\Omega_m = 0.26, w = -1.5$, the stretch of structure leads to shallower slope of $\hat{r}\xi$ and, the higher the redshift, the shallower. In all cosmologies we find significant detection of redshift evolution of $\hat{r}\xi$ (in the lowest panels, $\delta \hat{r}\xi \neq 0$). We computed the χ^2 values according to Equation 6 and found these sets of cosmological parameters are strongly disfavored at $\gtrsim 30\sigma$ CL.

5. COSMOLOGICAL CONSTRAINT

We constrain Ω_m and w through Bayesian analysis ((Christensen et al. 2001); also see (Lewis & Bridle 2002; Li et al. 2016) for details). We assue the likelihood takes the form

$$\mathcal{L} \propto \exp \left[-\frac{\chi^2}{2} \right] \quad (8)$$

and scan the parameter space in $\Omega_m - w$ plane to obtain the 68.3% and 97.4% CL regions. The result is displayed in Figure ??.

We get tight constraint on the two paramters. The 2σ contour lies within the region $0.23 < \Omega_m < 0.285$, $-1.1 < w < -0.9$. The thin shape of contour means, when combining with the another observational data with different direction of degeneracy (e.g. CMB), very tight combined constraint can be obtained. In case of fixing one parameter at its best-fit value and infer the

² The error bars displayed in all figures are estimated from the 120 subsamples and for the error bar of redshift evolution of 2pCF we always take the cosmic variance into consideration.

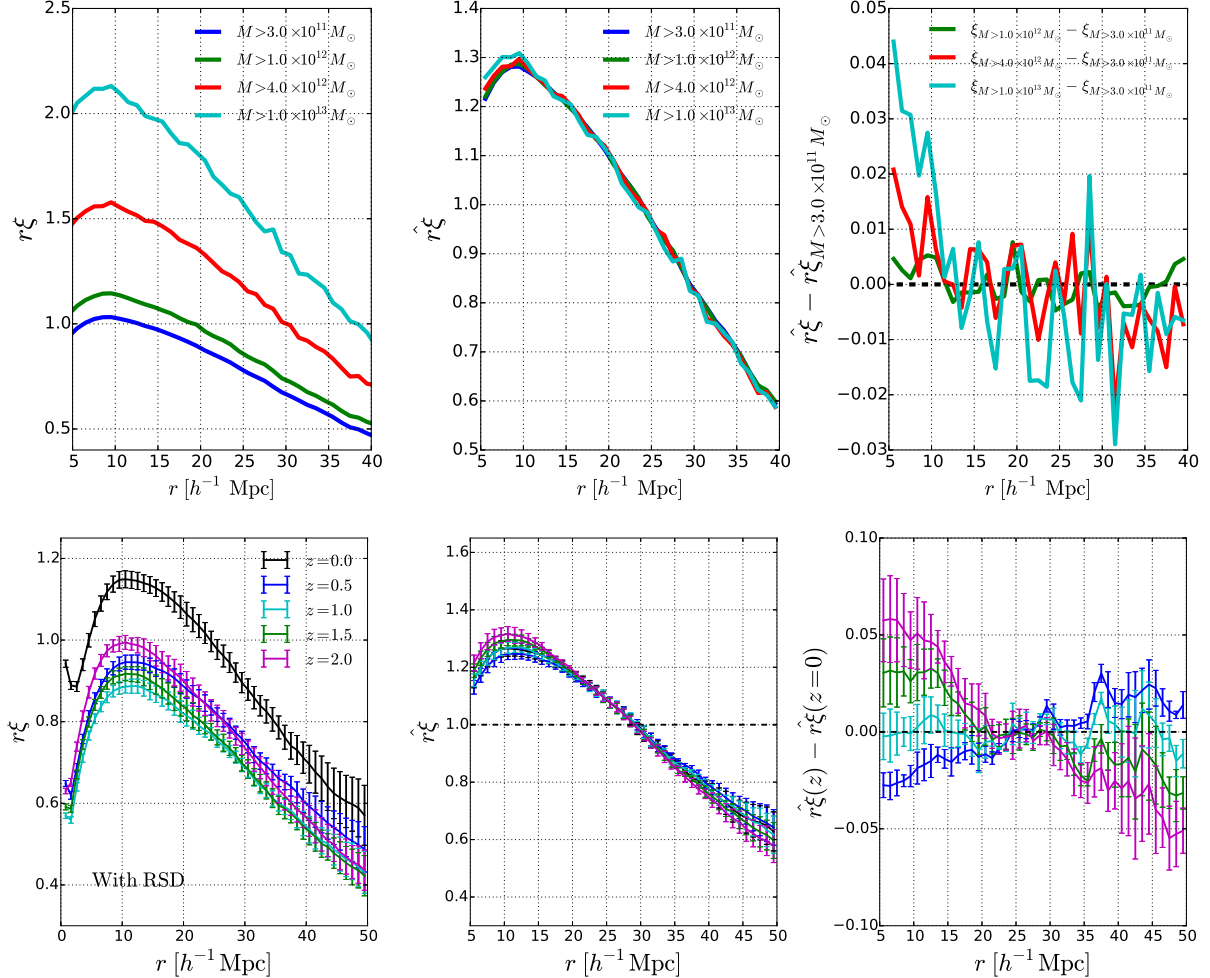


Figure 4. Systematic effects.

statistical uncertainty of the other one, one will obtain 1σ uncertainty of $\delta\Omega_m \approx 0.002$, $\delta w \approx 0.01$.

6. CONCLUDING REMARKS

* Can be combined with our redshift dependence of AP to full explore the geometric effects in LSS

* *** utilizes angular 2pCF as a function of redshift. Our method is complementary to it: 1) smaller scales; 2) more bins; 3) could be less affected by RSD; ... In case of good modelling of RSD one can rely on their; in case not possible, especially on small scales, one can use ours

* Complementary to all other LSS probes

* Promising future

ACKNOWLEDGMENTS

We thank the Korea Institute for Advanced Study for providing computing resources (KIAS Center for Advanced Computation Linux Cluster System). We would like to thank Yi Zheng for useful discussions. This work was partially supported by the Supercomputing Center/Korea Institute of Science and Technology Information with supercomputing resources including technical support (KSC-2013-G2-003).

APPENDIX

REFERENCES

- Ade, P.A.R., Aghanim, N., & Arnaud, M., et al. arXiv:1502.01589
- Alam, S., Ata, M., & Bailey, S., et al. 2016, submitted to MNRAS (arXiv:1607.03155)
- Alam S., Albareti, F.D., & Allende Prieto, C., et al., 2015, ApJS, 219, 12
- Alcock, C., & Paczynski, B. 1979, Nature, 281, 358
- Anderson, L., Aubourg, É., & Bailey, S. et al. 2014, MNRAS, 441, 24
- Ballinger, W.E., Peacock, J.A., & Heavens, A.F. 1996, MNRAS, 282, 877
- Betoule, M., Kessler, R., & Guy, J., et al. 2014, A&A, 568, 32
- Beutler, F., Blake, C., & Colless, M., et al. 2011, MNRAS, 416, 3017
- Beutler, F., Saito, S., & Seo, H.-J., et al. 2013, MNRAS, 443, 1065
- Beutler, F., Seo, H.-J., & Saito, S., et al. 2016, arXiv:1607.03150
- Blake, C., Glazebrook, K., & Davis, T. M., 2011, MNRAS, 418, 1725
- Blake, C., James, J.B., & Poole, G.B. 2013, MNRAS, 437, 2488
- Bolton, A.S., Schlegel, & D.J., Aubourg E., et al. 2012, AJ, 144, 144
- Boylan-Kolchin, M., Ma, C.-P., & Quataert, E. 2008, MNRAS, 383, 93
- Christensen, N., Meyer, R., Knox, L., & Luey, B. 2001, Class. Quant. Grav., 18, 2677
- Chuang, C.-H., & Wang, Y. 2012, MNRAS, 426, 226

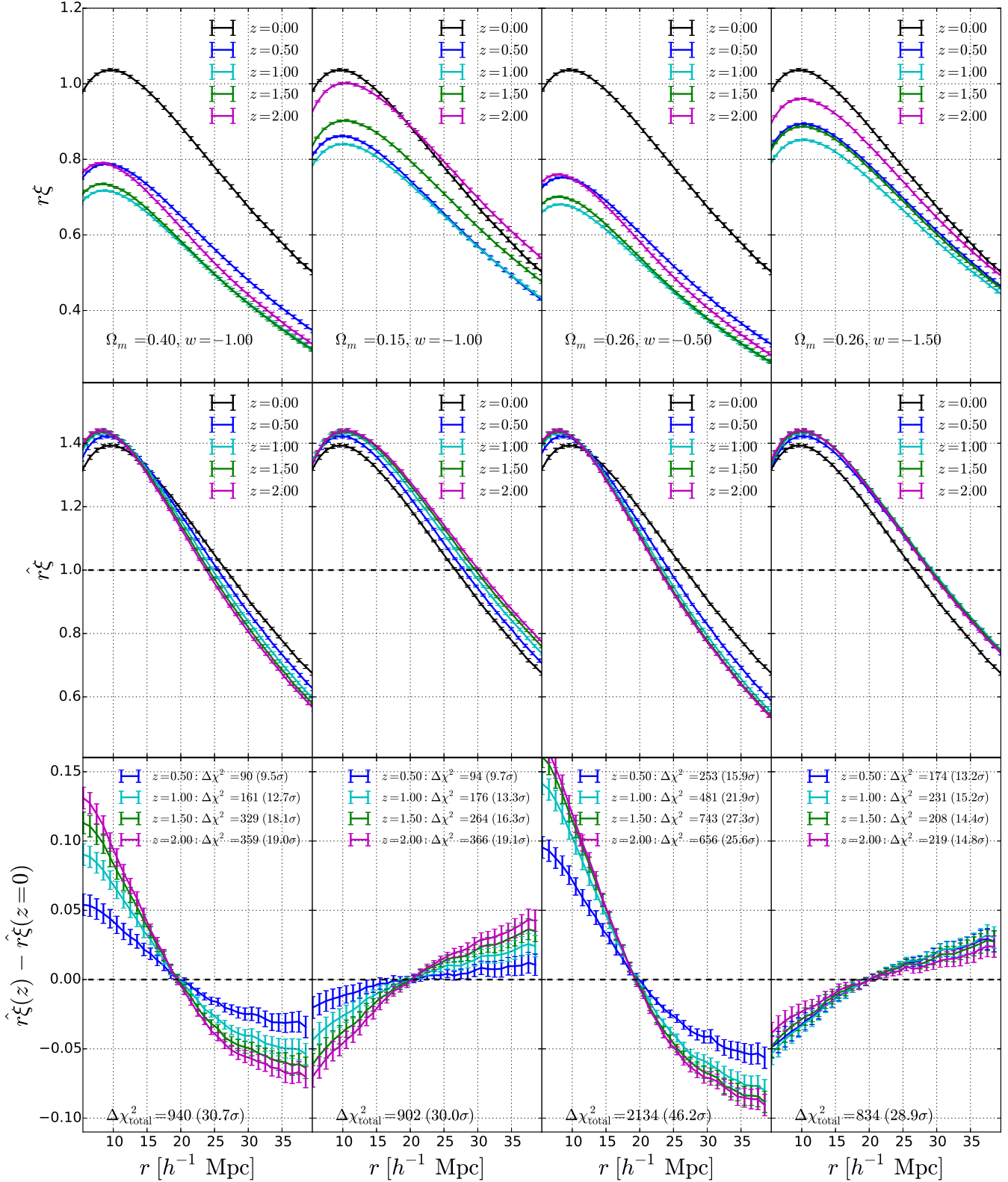


Figure 6. Likelihood contours (68.3%, 95.4%) in the $\Omega_m - w$ plane from our method.

- Dawson, K.S., Kneib, J.P., & Percival, W.J., et al. 2015, accepted AJ
- Dawson, K.S., Schlegel, D.J., & Ahn, C.P., et al. 2012, AJ, 145, 10
- Efstathiou, G. 2014, MNRAS, 440, 1138
- Eisenstein, D.J., Weinberg, D.H., & Agolet, E., et al. 2011, AJ, 142, 72
- Feldman, H.A., Kaiser, N., & Peacock, J.A. 1994, ApJ, 426, 23
- Fukugita, M., Ichikawa, T., & Gunn, J.E., et al. 1996, AJ, 111, 1748
- Gunn, J.E., Carr, M., & Rockosi, C. et al. 1998, AJ, 116, 3040
- Gunn, J.E., Siegmund, W.A., & Mannery, E.J., et al. 2006, AJ, 131, 2332
- Guzzo, L., Pierleoni, M., & Meneux, B., et al. 2008, Nature, 451, 541
- Hartlap J., Simon P. & Schneider P. [astro-ph/0608064].
- Hong, S.E., Park, C.,& Kim, J. 2016, ApJ, 823, 103
- Jackson, J., 1972, MNRAS, 156, 1
- Jennings, E., Baugh, C.M., & Pascoli, S. 2011, MNRAS, 420, 1079
- Jiang, C.Y., Jing, Y. P., & Faltenbacher, A., et al. 2008, ApJ, 675, 1095
- Kaiser, N. 1987, MNRAS, 227, 1
- Kim, J., & Park, C. 2006, ApJ, 639, 600
- Kim, J., Park, C., Gott, J.R., III, & Dubinski, J. 2009, ApJ, 701, 1547
- Kim, J., Park, C., L'Huillier, B., & Hong, S. E. 2015, JKAS, 48, 213
- Kim, J., Park, C., Rossi, G., Lee, S.M., & Gott, J.R. 2011, JKAS, 44, 217
- Kitaura, F.S., Rodríguez-Torres, S., Chuang, C.-H., et al. arXiv:1509.06400
- Komatsu, E., Smith, K. M., & Dunkley, J., et al. 2011, ApJS, 192, 18
- Lacey, C., & Cole, S. 1993, MNRAS, 262, 627
- Landy, S.D., & Szalay, A.S. 1993, ApJ, 412, 64
- Laureijs, R., Amiaux, J., & Arduini, S., et al. 2011, arXiv:1110.3193
- Lavaux, G., & Wandelt, B.D. 2012, ApJ, 754, 109
- Lewis, A., & Bridle, S. 2002, Phys. Rev. D, 66, 103511
- L'Huillier, B., Park, C., & Kim, J. 2014, New Astronomy, 30, 79
- Li, M., Li, X.-D., Wang, S., & Wang, Y. 2011, Commun. Theor. Phys., 56, 525
- Li, X.-D., Park, C., Forero-Romero, J., & Kim, J. 2014, ApJ, 796, 137
- Li, X.-D., Park, C., Sabiu, C.G., & Kim, J. 2015, MNRAS, 450, 807
- Li, X.-D., Park, C., Sabiu, C.G., & Kim, J. 2016, submitted to ApJ
- Linder, E.V., Minji, O., Okumura, T., Sabiu, C.G., & Song, Y.-S. 2014, Phys. Rev. D, 89, 063525
- López-Corredoira, M. 2014, ApJ, 781, 96
- Marinoni, C., & Buzzi, A. 2010, Nature, 468, 539
- Matsubara T., & Suto, Y. 1996, ApJ, 470, L1
- McCavanaugh, T., Micic, M., Lewis, G. F., et al. 2012, MNRAS, 424, 361
- Morandi, A., & Sun, M. arXiv:1601.03741
- Outram, P.J., Shanks, T., Boyle, B.J., Croom, S.M., Hoyle, F., Loaring, N.S., Miller, L., & Smith, R.J. 2004, MNRAS, 348, 745
- Parejko J.K., et al., 2013, MNRAS, 429, 98
- Parihar, P., Vogeley, M.S., & Gott, J.R., et al. 2014, ApJ, 796, 86
- Park, C., Kim, J., & Gott, J.R. 2005, ApJ, 633, 1
- Park, C., & Kim, Y.-R. 2010, ApJL, 715, L185
- Park, C., Choi, Y.-Y., Kim, J., Gott, J.R., Kim, S.S., & Kim, K.-S. 2012, ApJ, 759, 7
- Park, C., Song, H., Einasto, M., Lietzen, H., & Heinamaki, P. 2015, JKAS, 48, 75
- Peebles, P.J.E., & Ratra, B. 2003, Reviews of Modern Physics, 75, 559
- Percival, W.J., Ross, A.J., & Sánchez, A.G., et al. 2014, MNRAS, 439, 2531
- Perlmutter, S., Aldering, G., & Goldhaber, G., et al. 1999, ApJ, 517, 565
- Press, W.H., & Schechter, P.L. 1974, ApJ, 187, 425
- Reid, B., Samushia, L., & White, M., et al. 2012, MNRAS, 426, 2719
- Reid, B., Ho, S., & Padmanabhan, N., et al. 2016, MNRAS, 455, 1553
- Riess, A.G., Filippenko, A.V., & Challis, P., et al. 1998, AJ, 116, 1009
- Riess, A.G., Macri, L., & Casertano, S., et al. 2011, ApJ, 730, 119
- Ross, A.J., Percival, W.J., & Sánchez, A.G. et al. 2012, MNRAS, 424, 564
- Ross, A.J., Samushia, L., & Howlett, C., et al. 2015, MNRAS, 449, 835
- Ryden, B.S. 1995, ApJ, 452, 25
- Sanchez, A. G., Scoccimarro, R., & Crocce, M., et al. arXiv:1607.03147
- Schlafly E.F., Finkbeiner D.P., Schlegel D.J., et al. 2010, ApJ, 725, 1175
- Schlafly E.F., & Finkbeiner D.P. 2011, ApJ, 737, 103
- Schlegel, D., Abdalla, F., & Abraham, T., et al. 2011, arXiv:1106.1706
- Smee, S.A., Gunn, J.E., & Uomoto, A., et al. 2013, AJ, 146, 32
- Song, Y.S., Sabiu, C.G., Okumura, T., Oh, M., & Linder, E.V. 2014, JCAP, 12, 005
- Speare, R., Gott, J.R., Kim, J., & Park, C. 2015, ApJ, 799, 176
- Viana, P.T.P., & Liddle, A.R. 1996, MNRAS, 281, 323
- Villalobos, Á., De Lucia, G., Weinmann, S.M., Borgani, S., & Murante, G. 2013, MNRAS, 433, L49
- Weinberg, S. 1989, Reviews of Modern Physics, 61, 1
- White M., et al. 2011, ApJ, 728, 126
- York, D.G., Adelman, J., & Anderson, J.E., et al. 2000, AJ, 120, 1579
- Zehavi, I., Zheng, Z., & Weinberg, D.H., et al. 2011, ApJ, 736, 59